

Do Cooling Flows Survive Cluster Mergers?

P. L. Gómez¹

*Dept. of Physics & Astronomy, Rutgers The State University of New Jersey,
136 Frelinghuysen Road, Piscataway NJ 08854-8019,
Email: percy@physics.rutgers.edu*

C. Loken^{1,2}, K. Roettiger, J. O. Burns¹

*Dept. of Physics & Astronomy, University of Missouri - Columbia,
Columbia MO 65211,
Email: cloken@ap.stmarys.ca, kroett@hades.physics.missouri.edu, burnsj@missouri.edu*

ABSTRACT

We report the results of recent numerical simulations of the head-on merger of a cooling flow cluster with an infalling subcluster of galaxies. The objective of these simulations was to examine the effects of different types of cluster mergers (with 16:1 and 4:1 mass ratios) on the evolution of cluster cooling flows (with mass accretion rates of 100 and 400 M_{\odot} /year). The 2-dimensional simulations were performed with a combined Hydrodynamics/N-body code on a uniform grid with a resolution of 20 kpc (~ 12 zones/core radius).

In our simulations, cooling flow disruption is indicated by a dramatic increase (by a factor of 10-40) in the central cooling time of the primary cluster. We find that the ram-pressure of the infalling gas is crucial in determining the fate of the cooling flow as disruption occurs when a substantial amount of subcluster gas reaches the primary's core. In such cases, the subcluster gas can increase the central cooling time by displacing the high-density cooling gas and by heating it via shocks and turbulent gas motions. However, the fate of a merging cooling flow is also dependent on its initial cooling time. In cases where the initial cooling time is very small (i.e., 10-40 times smaller than the Hubble time) then, even if the flow is disrupted, the central cooling time will remain less than a Hubble time and the flow will likely re-establish itself. This has an important observational consequence because such clusters will be classified as cooling flows on the basis of their cooling times even though they have experienced a significant merger. In addition, we find that there is a time delay between core-crossing and the point at which the central cooling time of a disrupted flow becomes of order a Hubble time. Thus, even in the case of disruption, a cluster can be classified as a cooling flow and exhibit substructure (indicative of a merger) for 1-2 Gyr after merging with a subcluster. We argue that our results make it possible to reconcile the high cooling flow frequency

¹Much of the work reported here was performed while at the Department of Astronomy, New Mexico State University, Las Cruces, NM

²present address: Dept. of Astronomy & Physics, Saint Mary's University,
Halifax, NS, B3H 3C3, Canada

inferred by some observations with both high merger rates and a high frequency of substructure.

Subject headings: galaxies: clusters — intergalactic medium — X-rays: galaxies

1. INTRODUCTION

Clusters of galaxies form at the intersection of sheets and filaments in the “Cosmic Web” through a process of accretion and mergers with other clusters (e.g., Bond, Kofman, & Pogosyan 1996; Colberg et al. 1999). Thus, mergers are very likely a generic element of cluster evolution. Their effects on cluster morphologies and properties (e.g., Burns 1998) have been investigated via high-resolution numerical simulations which reproduce many of the features in observed merger candidates (e.g., Evrard et al. 1993; Roettiger, Burns & Loken 1996, Roettiger, Stone & Mushotzky 1998). Numerical simulations are essential for understanding the details of cluster physics and evolution as well as for interpreting observations which attempt to use clusters in order to constrain cosmological parameters (e.g., Gunn 1978; Birkinshaw 1979; Richstone et al. 1992; Mohr et al. 1995).

Another common feature of cluster evolution appears to be the formation of cooling flows (e.g., review by Fabian 1994). A large fraction ($> 50\%$ of x-ray bright clusters; e.g., Edge, Stewart, & Fabian 1992; White, Jones, & Forman 1997; Edge 1997) of massive clusters are believed to harbor cooling flows which may be the natural outcome of cluster evolution over a wide range in cluster masses (Knight & Ponman 1997). A cooling flow evolves in a cluster atmosphere because the X-ray emission is a very effective cooling mechanism. The typical physical properties of the gas located at the core of a cooling flow cluster (i.e., $n \sim 0.01 \text{ cm}^{-3}$ and $T \sim 10^7 \text{ K}$) imply a cooling time less than the age of the Universe. Therefore, gas surrounding this core, which cannot cool as fast as the central gas, loses pressure support and starts a subsonic inward flow. Note that most of the evidence supporting the presence of cooling flows in galaxy clusters is indirect because current X-ray telescopes lack the spectral resolution to directly measure velocities via emission lines. Thus, cooling flows are inferred to exist from observed cluster gas temperature gradients (e.g., White & Silk 1980; Allen et al. 1995), from the detection of excess emission in the cluster core (e.g., Stewart et al. 1984; Allen et al. 1995), or from the presence of $\sim 10^4 \text{ K}$ gas in cluster cores as revealed by observations of $\text{H}\alpha$ filaments (Heckman et al. 1989; Donahue et al. 1992; Crawford et al. 1995).

Is there any correlation between the presence of cooling flows and the presumed merger history of a cluster? Donahue et al. (1992) found evidence of more

cooling flow clusters in the past than in the present by studying their optical $\text{H}\alpha$ emission. In their analysis, the percentage of cooling flow clusters increases to 56% in the redshift range $0.2 < z < 0.37$ from 35% in the $0.065 < z < 0.14$ range. This result can be explained if mergers are more frequent in the present than in the past *and* if cluster mergers disrupt cooling flows. However, this putative increase in cooling flow frequency with redshift is contradicted by Crawford et al. (1995) who analyzed a sample of 20 clusters with $z > 0.2$ and concluded that only 35% of them show evidence of $\text{H}\alpha$ emission. To complicate matters even more, the suggestion that there are relatively few nearby cooling flow clusters has been questioned since some observations suggest that as many as (70-90)% of bright nearby clusters have cooling flows (e.g., Edge, Stewart, & Fabian 1992; White, Jones, & Forman 1997; Peres et al. 1998) with 39% of them showing optical line emission (Edge & Stewart 1991).

Detailed multiwavelength observations of some galaxy clusters seem to support the hypothesis that cluster mergers affect and in some cases even destroy cluster cooling flows. The presence of X-ray and/or optical substructure is used to infer a dynamically complex system and/or a recent cluster merger where the gas is not in hydrostatic equilibrium with the gravitational potential (Davis & Mushotzky 1993, White et al. 1993, Mohr et al. 1993). The Coma cluster (e.g., Burns et al. 1994), A2256 (e.g., Briel & Henry 1994; Roettiger, Burns, & Pinkney 1995; Markevitch 1996), A2255 (Burns et al. 1995) and A3627 (e.g., Böhringer et al. 1996) are some examples of massive clusters that appear to have undergone a recent merger but do not have cooling flows. On the other hand, A1664 (Allen et al. 1996), A2597 (Sarazin et al. 1995, Gómez et al., in preparation), A2390 and A2667 (Rizza et al. 1998), and A2065 (Markevitch et al. 1999) are examples of clusters with evidence for both a cooling flow *and* x-ray substructure. All these results may make sense in view of the relation between cluster substructure and cluster cooling flow strength uncovered by Buote & Tsai (1996) in a study of 23 clusters. They quantified the dynamical state of a cluster and its substructure by using a power ratio technique that consists of expanding the cluster X-ray surface brightness into gravitational multipoles. In this manner, they find that the ratio of quadrupole-to-monopole (a measure of cluster substructure) decreases as the cooling flow strength increases. Their findings are consistent with

a scenario in which recent mergers can either diminish the strength of a cooling flow (e.g., A1664) or even destroy them (e.g., Coma, A2256). If we assume that the substructure was created by a recent cluster merger (and the substructure has a lifetime short compared to the time necessary to re-establish a disrupted cooling flow), then mergers may not always destroy the cluster cooling flow.

Despite the apparent ubiquity of both the cooling flow phenomenon and mergers, no detailed numerical studies of the effects of mergers on cooling flows have been performed to date. Early N-body simulations with no gaseous component (McGlynn & Fabian 1984) and more recent analytic studies (Fabian & Daines 1991) have suggested that mergers destroy cooling flows but these studies have limitations (for example, Fabian & Daines considered only subsonic mergers between clusters of roughly equal mass) that prevent applying their results to the wide range of parameters (masses, cooling flow strengths etc.) which characterize actual mergers. For instance, the typical cluster gas sound speed is $\sim 1,000 \text{ km s}^{-1}$ while the free-fall relative velocity between the merging clusters could be as high as $3,000 \text{ km s}^{-1}$. These estimates are consistent with the values derived by Markevitch et al. (1998b) in Cygnus A, A3667, and A2065. Therefore, this is a complex problem that needs the more sophisticated treatment provided by numerical simulations.

In order to study the effects that cluster mergers have on cooling flows, we have performed a set of new 3D N-body with 2D Hydro numerical simulations (assuming cylindrical symmetry and with 20 kpc resolution) of head-on cluster mergers in which we follow the evolution of a cooling flow located in the most massive cluster (i.e., the primary cluster). With this study, we propose to answer the following questions: (1) What type of merger affects a cluster cooling flow? and (2) If a cooling flow is disrupted (i.e., the core is heated and the cooling time increases), what are the merger parameters that determine if a new cooling flow can be formed?

We have organized this paper as follows. In §2, we describe the code used in the simulations, the initial conditions, as well as some of the code tests. Section 3 presents the general results from all the simulations. Next, we discuss the possible interpretations of the numerical simulations in §4. Finally, we summarize our conclusions in §5. We use $H_0=75 \text{ km/s/Mpc}$ and $q_0=0.5$ throughout the paper.

2. NUMERICAL METHOD

All the simulations presented here were performed with a hybrid code similar to the one used by Roettiger et al. (1993, 1996, 1997) that combines the N-body code TREECODE (Hernquist 1987; with a softening parameter of 0.2 and a tolerance of 0.7) with the Eulerian, finite-difference fluid dynamics code ZEUS-3D (Clarke 1990; Stone & Norman 1992). The main differences between our code and Roettiger et al.'s code are that (1) we increased the resolution by a factor of 2.5 by performing these simulations in 2 dimensions and invoking cylindrical symmetry along the merger axis, (2) we used a different Poisson solver for computing the gravitational potential from the N-body particles, and (3) we included radiative cooling.

The only link between the hydro and N-body codes is through the Poisson solver. Every time an N-body step is required, the evolving 3-D N-body particles are rebinned in 2-D. Next, we determine the boundary conditions by computing the contribution of each particle at every boundary cell. Finally, we solved the finite-differenced Poisson equation in 2-D by using the Generalized Conjugate Residual method (GCR; Eisenstat et al. 1983) within the NonSymmetric PreCondition Gradient package (NSPCG; Oppe et al. 1988). Typically, there are 5-7 hydro time steps (governed by the Courant condition) for every N-body step. Our implementation of the code does not include the self-gravity of the gas which is not expected to be important since the gas component comprises less than $\sim 15\%$ of the total dynamical mass.

The cooling function that we used is an analytical approximation to the cooling curve (Raymond & Smith 1977) based on the equations given by Westbury & Henriksen (1992) for the case of half-solar abundance. Our modeling of the effects of radiative cooling is computationally expensive because it includes the solution of the energy equation in every cell at every time step. We avoid the problem of catastrophic cooling at the cluster core with the use of a mass drop-out term intended to simulate the mass loss produced by star formation. This term follows the prescription of Sarazin and White (1985) for mass loss ($d\rho/dt = q\rho/t_c$, where q is the mass drop out term and t_c is the cooling time). Unfortunately, this extra term forces us to solve the continuity and energy equations as two coupled implicit equations by using the Newton-Raphson method. However, the use of 2D cylindrical symmetry allows us to perform these

simulations with significant savings in the run time. Note that the amount of gas that drops out during the entire simulation is gravitationally negligible (less than 2.5% of the total core mass).

In order to follow the evolution of the primary and secondary cluster gas during the merger, we have added two passive (i.e., dynamically insignificant) scalars (or tracers) to the code. Each cluster was initialized with a passive scalar distribution that mimicked its initial cluster gas distribution. As the simulation progressed, the passive scalars were advected by the velocity field. In this way, we were able to trace the motion of each cluster’s gas during the merger.

In order to test and verify our new code, we performed the same cluster tests used by Roettiger et al. (1997) which consisted of evolving a cluster composed of only N-body particles, N-body particles and gas, and the uniform motion of an isothermal cluster composed of N-body particles and gas across the grid. We found excellent agreement between these tests. We also verified that we could move an isolated cluster with a steady-state cooling flow across the grid at 600 km/s with no major changes in the cooling time, the central temperature, or in the radial density profile. This test is essential to our demonstration (§3.3) that some mergers are able to disrupt a cooling flow.

2.1. Parameter Space

McGlynn and Fabian (1984) suggested that a merger of two similar clusters would destroy a cluster cooling flow. Indeed, recent numerical simulations (most without radiative cooling and none with cooling flows) performed by various groups (e.g., Roettiger et al. 1993, 1996; Schindler & Müller 1993; Pearce, Thomas, & Couchman 1994) have shown that these massive mergers have profound effects on the properties of the cluster gas. For instance, these mergers generate large gas bulk flow motions and turbulence, especially, within the core. Thus, we decided to study the effects of mergers with lower mass subclusters since we assumed that mergers between similar clusters (mass ratio of 1:1 or 2:1) would very likely destroy cooling flows.

The first parameter that we explored was the total mass of the subcluster. The sudden inflow of the subcluster will cause a rapid fluctuation of the gravitational potential that could affect the cluster cooling flow region. For our simulations, we have chosen a

primary cluster with a dark matter mass of $10^{15} M_{\odot}$ (i.e., Coma-like) and subclusters with 1/16 ($0.625 \times 10^{14} M_{\odot}$) and 1/4 ($2.5 \times 10^{14} M_{\odot}$) the primary cluster mass (see Table 1).

The amount of gas in the infalling secondary cluster is also likely to be an important parameter. Increasing the baryon fraction in the secondary cluster will increase the ram-pressure of the infalling gas which, if it reaches the primary core, may have significant dynamic or thermal effects on the cooling flow. Thus, we address the question of whether gas-rich subclusters are more likely to affect the primary cooling flow than gas-poor subclusters by varying the gas mass fraction in the subcluster from 1.2% to 15%. We did not attempt to go higher than 15% because our code does not include gas self-gravity. Note that poor clusters typically have low gas fractions ($\sim 5\text{--}30\%$ Mulchaey et al. 1996).

The last parameter varied was the strength of the cooling flow (i.e., \dot{M} or the mass accretion rate). We chose two primary cluster cooling strengths: 100 and 400 M_{\odot}/year . We hypothesized that a stronger cooling flow should be more difficult to destroy by a merger than a weak cooling flow. This is because a stronger cooling flow would have a very steep central density profile, and thus, it would be more likely to dissipate the effects of the shock formed during the merger. Table 1 shows the parameter combinations used in our simulations.

2.2. Initial Conditions

The initial conditions for the simulations were simple and idealized. We started with a massive primary cluster with a cooling flow and an isothermal secondary cluster that merge under the influence of their mutual gravity. They were placed on a cylindrical grid with dimensions 500 x 150 zones (assuming azimuthal symmetry) corresponding to a resolution of 20 kpc per zone (~ 12 zones across the primary cluster core radius) and given an initial relative velocity of 600 km/s which is consistent with the mean peculiar velocity of nearby galaxy clusters (Colless et al. 1999). The initial separation between the clusters was 4.9 Mpc for the 1:4 mass ratio mergers and 4.4 Mpc for the 1:16 mass ratio mergers. This setup has two advantages. First, it puts the clusters far enough apart so that they do not severely affect each other. Second, the clusters are close enough so that the merger occurs fairly quickly, thus, saving computational time.

There are several advantages in using these simplified initial conditions (e.g., Roettiger et al. 1993; 1997, Pearce et al. 1994) over cosmological initial conditions. First, the use of already formed clusters allows us to use a relatively small grid, thus, enhancing the spatial resolution. Second, the symmetry of the set-up allows us to perform the gas simulations in 2D which saves run time and memory requirements. Finally, we have a very well defined baseline with which to compare the subsequent evolution making it straightforward to determine how the cluster properties are affected by the merger.

The collisionless dark matter was represented by N-body particles distributed spatially according to a lowered isothermal King model (King 1966) characterized by a concentration parameter of 1.08 (Binney & Tremaine 1987). The primary cluster dark matter in each simulation was represented by 30,000 N-body particles whereas the number of particles in the secondary clusters was scaled accordingly so that each N-body particle has the same mass. Table 1 includes the number of particles per subcluster.

The secondary cluster gas was initially isothermal and in hydrostatic equilibrium with its dark matter gravitational potential. Thus, the shape of the gas distribution (we assume $\beta = 1.0$) and the gas temperature were obtained by solving the equation of hydrostatic equilibrium. This approach leaves the central density of the secondary cluster as a free parameter. However, our choice for the central density was limited by the fact that we do not include self-gravity in the code; thus, we chose an overall gas fraction $\leq 15\%$. This choice also assures us that the central cooling time for the subcluster is much larger than a Hubble time. Other cluster parameters appear in Table 1.

The cooling flow cluster was assembled in a different manner. First, we computed the gravitational potential produced by the primary cluster dark matter distribution. Next, we laid down an isothermal gas distribution in hydrostatic equilibrium with this gravitational potential onto the ZEUS grid. Then, we turned on cooling and followed the evolution of the cluster core until it reached a steady-state cooling flow (this process normally takes ~ 5 -7 cooling times). Table 2 shows the initial parameters of the pre-cooling flow isothermal clusters used in the cooling flow model evolution. In order to avoid the problem of catastrophic cooling at the cluster core and as a way to represent the multiphase nature of the

cooling gas, we used a mass drop-out value of 0.2 in the simulations ($q_{drop} = 0.2$; Westbury & Henriksen 1992). Finally, we extracted the 1D density, temperature, and radial velocity profiles and used them as the initial conditions for the primary cluster cooling flow. The two steady-state cooling flows were measured to have mass accretion rates (\dot{M}) of 100 and 400 M_{\odot} /year at the cooling radius (where the cooling time is equal to the age of the Universe). Figure 1 shows the density and temperature profile of our cooling flow models. Note that the central region of the cluster (< 100 kpc) has a lower temperature and a higher gas density than the surrounding cluster gas.

3. RESULTS

3.1. Dark Matter Evolution

As has been pointed out before (e.g., Roettiger et al. 1997), the most important effect due to the dark matter evolution is the sudden fluctuation of the gravitational potential minimum during core crossing. Figure 2, which shows the evolution of the gravitational potential minimum as a function of the time, confirms that the most dramatic change occurs during core crossing in the 4:1 mass ratio cluster merger. At this time, the gravitational potential suffers a sudden and relatively brief (~ 1 Gyr in duration) deepening caused by the subcluster. Moreover, the oscillations in the gravitational potential, which are caused by the secondary cluster falling back into the primary cluster, suggest that the secondary cluster dark matter distribution survives the first pass through the primary cluster core. On the other hand, the lack of gravitational potential oscillations and the presence of a spray of N-body particles exiting the primary cluster points toward the destruction of the secondary cluster during the 16:1 merger. Note that the most dramatic changes in the gravitational potential, which should cause mixing and heating of the gas, occur in the 4:1 mass ratio merger. Are these changes strong enough to affect the gas properties of the cooling flow region? We will address this question in §4.

3.2. Cluster Gas Evolution

In general, the evolution of the cluster gas in our nine merger simulations follows the same patterns described in the analysis of other numerical simulations (e.g., Roettiger et al. 1993, 1997; Schindler & Müller 1993; Pearce et al. 1994). To facilitate our explanation of the effects of mergers on cooling flows, we

will concentrate on the gas evolution in two simulations: #7 and #8 (Table 1). These simulations are both 16:1 mass ratio mergers involving identical cooling flow clusters and differ only in the secondary cluster’s total gas content. We chose these two examples because the cooling flow (e.g., central region of low temperature and high density) survives the effects of the merger #7 while it is disrupted in merger #8.

Figure 3 consists of 6 contour plots showing the evolution of the logarithm of the gas density in merger #8 (Table 1). The density contours are overlaid onto a grey scale plot that represents the distribution of the secondary cluster passive scalar (§2) which traces the secondary cluster gas. Note that the times are relative to the core passage and that in all the panels the contours and grey levels are scaled to the same values. In the first two panels, we see the subcluster falling towards the primary cluster from the right and creating a bimodality in the gas density distribution. The leading edge of the subcluster is compressed and develops into a bow shock as the subcluster’s motion soon becomes supersonic (at ~ 0.6 Gyrs before core crossing).

The morphological effects of the merger are most strongly evident at the time of core crossing and shortly thereafter. For instance, the primary cluster core suffers several changes as it evolves from being spherical before core-crossing to an elliptical shape at $t=0$. Later, the core exhibits extreme isophotal twisting ($t=0.25$ Gyrs) which relaxes back into an elliptical core ($t=1$ Gyrs). Eventually, the merger remnant will re-adopt a more circular shape ($t \sim 5.5$ Gyrs). The most interesting morphology occurs at $t=0.25$ Gyrs when the core (inner ~ 200 kpc) of the cluster shows two distinct elongations in the density distribution. One elongation is parallel to the merger axis and is likely caused by the reaction of the cluster gas to an elongated gravitational potential which is aligned along the merger axis. This elongation forms slightly before the time of core crossing and lasts at least 1 Gyr. The second elongation is perpendicular to the merger axis, lasts for 0.75 Gyrs, and is 500 kpc wide. The grey scale plot suggests that this elongation is caused by compressed secondary cluster gas that is mixing with and impinging on primary cluster gas.

Interestingly, the bow shock that appears at the leading edge of the secondary cluster gas distribution protects the subcluster gas from significant mixing with the primary cluster gas until $t=0.25$ Gyrs.

Note that the secondary gas was effectively stripped from its potential earlier (the subcluster DM passes through the primary cluster core at 0 Gyr). However, at $t=1$ Gyr, secondary cluster gas has started to penetrate the primary cluster core and by $t=5.5$ Gyrs, gas from the secondary cluster is readily mixing with primary cluster gas as can be seen in Figure 4. This figure shows line plots (along the merger axis) of the total gas density and the subcluster passive scalar at three different epochs.

Figure 5 depicts the same quantities and epochs as Figure 3 but for merger #7. There are two main differences in the gas evolution between these two mergers. First, the bimodality of the pre-merger gas distribution in merger #7 is not as evident as in merger #8. This is simply a reflection of the fact that the secondary cluster gas distribution is not as dense in #7 as it was in merger #8. Second, subcluster gas penetrates more deeply into the primary cluster core, and in greater amount, in merger #8 (see Figure 4). Note that at $t=5.5$ Gyrs, secondary cluster gas is present at the core of the primary cluster in both simulations; however, the density of the secondary cluster gas located within the cooling flow core is greater in merger #8 than in #7 as seen in Figure 4 (by almost a factor of 2).

Figures 3 and 5 also allow us to track the evolution of the cooling flow through the mergers. We can identify the cooling flow region as the very dense knot located at the primary cluster core. Note that at $t=5.5$ Gyrs, the primary cluster core in the gas rich secondary merger (#8, Figure 3) is less dense than it was before the merger (Figure 4). This demonstrates that the cooling flow properties have been affected by the merger. Moreover, the core of this cluster has expanded significantly due to heating and non-thermal pressure support (i.e., turbulence). This can be seen by analyzing Figure 4 and by comparing the evolution of the primary cluster core as depicted in the different panels in Figure 3. On the other hand, the primary cluster central density appears to remain unaffected throughout merger #7 (Figure 5).

3.3. Cooling Flow and Gas Temperature Evolution

The contour plots of the gas density evolution suggest that the properties of the cooling flow region were more strongly influenced by the high gas density subcluster (merger #8) than by the low gas density subcluster (merger #7). In order to expand this analysis

and determine how the merger has affected the gas temperature, we present a comparison of the temperature evolution for these two mergers.

Figure 6 shows grey scale plots of the evolution of the spatial distribution of the gas temperature for three epochs of simulations #7 and #8. Our analysis reveals a number of interesting features. First, there is evidence of the heating created by the bow shock that develops at the boundary between the two subclusters. We have examined this region of the cluster and determined that the strongest shock first appears at ~ 500 kpc from the primary cluster core and is generated by gas moving at peak Mach numbers $\sim 1-2$. Second, this shock penetrates deeper into the primary cluster for merger #8 (gas rich subcluster) than for merger #7. This suggests that the degree of penetration of the secondary cluster gas into the primary cluster depends on its relative momentum. We will discuss this possibility in more detail in the next section. Third, the cooling flow can be identified as the very cold (dark) region located at the center of the primary cluster in the first panel of these two figures. This cool region has all but disappeared at $t=5.5$ Gyrs in merger #8. The fact that the peak density in the primary cluster core has decreased while the minimum temperature has increased indicates that the cooling flow has been disrupted in this merger. Simulation #7 shows no such signatures and therefore the cooling flow has not been disrupted in this case.

This qualitative evidence for the disruption of the cooling flow can be quantified by reference to Figure 7 which shows the evolution of the cooling time in the primary cluster core. This figure clearly reveals the fate of the various cooling flow mergers we investigated. Mergers such as #8 show a dramatic increase in the cooling time after the merger while there is no change in the central cooling time for run #7. Since $t_{cool} \propto T^{1/2}/\rho$, any significant increase of the cooling time is an indication of an increase of the gas temperature and/or a decrease of the gas density. We have already noted that the central gas density decreases significantly in the case of disruption (run #8, see Figure 4). To assess the role of the temperature, we plot the evolution of the central gas temperature in Figure 8. The temperature evolution is remarkably similar to that of the cooling time but we note that the temperature change does not account for the entire change in t_{cool} . In fact, for merger #8, the density decrease (Figure 4) is more significant than the temperature increase in lowering the cooling time. Of course the

two effects are closely related as heating of the core will result in expansion and a lowering of the central gas density.

What are the crucial parameters which determine whether a merger will disrupt a cooling flow? The only clear trend is that the likelihood of disruption increases as the amount of gas in the secondary cluster increases. This behavior can be seen by considering mergers #1, #2, and #3 which differ only in the central density of the secondary cluster. There is strong disruption in the case where the secondary's central density is highest and only mild disruption in the others (see Fig. 7 and Table 1). The same trend can be seen in the case of a different mass ratio (#6 and #5) and in the case of a stronger cooling flow (#8, #7 and #9). It is difficult to discern, or even isolate, any systematic trends with cooling flow mass accretion rate or the mass ratio of the two clusters.

We find two interesting results which have consequences for reconciling observations of high cooling flow frequencies with high merger rates. First, we observe a time delay of typically 1-2 Gyrs between the time of core crossing and the time at which the cooling flow is disrupted (consider, e.g., mergers #6 and #4 in Fig. 7). Thus, even when the cooling flow will be strongly disrupted (e.g., merger #1), an observer could detect the signatures of substructure and a central cooling flow so long as the central cooling time is less than a Hubble time, i.e. for up to 2 Gyrs after the merger has taken place. As we will discuss later, this fact also supports the contention that gas dynamics (which will lag behind the N-body dynamics) accounts for the disruption of the cooling flow. Secondly, we point out that the fate of a cooling flow is dependent on its initial cooling time. In both mergers #6 and #8, the central cooling time rises by a factor of > 20 within 3 Gyrs of core-crossing indicating that the initial cooling flow has been disrupted. However, since the initial cooling time for merger #8 was very small (~ 0.1 Gyr), its final cooling time is still significantly less than a Hubble time and it would be observationally classified as a cooling flow. Thus, cooling flows with very short cooling times (≤ 0.2 Gyr), can be significantly affected by a merger yet still appear to be cooling flows. Furthermore, because the final cooling time is short, the original flow is likely to be quickly re-established in these cases.

4. DISCUSSION

4.1. What Destroys the Cooling Flow?

In the previous section, we showed that some types of cluster mergers are able to destroy cooling flows while other mergers will leave them intact. In this section, we will review some of the possible mechanisms triggered by a cluster merger that can affect the gas properties of the cooling flows.

One of these mechanisms is the violent increase in the depth of the gravitational potential at the time of core crossing. However, our analysis of the simulations indicates that this process is not the most important factor in determining the future of the cooling flow. For instance, we have shown that identical mass ratio mergers affect the cooling flow in different ways since we find a wide variety of outcomes in the 16:1 mass ratio mergers. Thus, there are no effects on the cooling flow produced by mergers #7 and #9 while the cooling flow does not survive merger #6. Furthermore, there is a delay between the moment of core crossing and when the cooling flow starts to feel the merger effects in our simulation (e.g., ~ 1.5 Gyrs in the case of merger #8). This delay suggests that the gravitational potential increase at the time of core crossing is not enough to destroy the cooling flow. Finally, in an effort to better isolate the effects of the gravitational potential from the effects caused by gas dynamics, we ran a 16:1 mass ratio merger (#9) of a cooling flow cluster with an essentially gas-free secondary cluster. We note that this merger does not significantly affect the gas properties of the cooling flow region. The different reaction of the cooling flow to the same mass ratio mergers is an indication that the most important mechanism responsible for disrupting the cooling flow is the interaction of primary and secondary cluster gas.

Another potential mechanism responsible for the disruption of the cooling flow region is shock heating of the gas. A shock is generated by the supersonic infall of the secondary cluster gas into the primary cluster core. For instance, the infalling secondary gas develops a Mach 2 shock when its leading edge is located at ~ 200 – 500 kpc from the primary cluster (e.g., merger #7). When the clusters are separated by less than 200 kpc, it is difficult to identify the shock structure due to the steep density profile near the core and in the cooling flow. Moreover, the shock decelerates as it moves closer to the core as it encounters an increase in the ambient density. Even if this Mach 2 shock were to penetrate all the way to the core of

the primary cluster, it would only increase the temperature by a factor of ~ 2.1 . This limited amount of heating could not cause the large central temperature jumps observed in mergers #1, #4, #6, and #8. However, this heating could explain the small disruption caused in other mergers (e.g., #3).

Our results support Fabian & Daines (1991) suggestion that the most important factor in determining whether a cooling flow can survive a merger is the ram pressure of the infalling secondary cluster. This could explain why mergers that differ only in the secondary cluster gas content have different effects on cooling flow evolution. In order to test this idea, we have compared the relative infall velocity of the secondary cluster (v_s) with a threshold velocity (v_{bal}). We define v_{bal} as the velocity that balances the cooling flow thermal pressure with the ram pressure produced by the motion of the subcluster gas (i.e., $v_{bal}^2 = P_{CF}/\rho_{sec}$, where P_{CF} is the primary cluster thermal pressure, and ρ_{sec} is the secondary cluster central density). The right-hand panel of Figure 9 shows a plot of v_{bal} as a function of radius for all of our 4:1 simulations while the left-hand panel shows the same plot for the 16:1 mass ratio mergers. Furthermore, we have overlaid on these plots (thick line) our estimate for the v_s of the secondary cluster. This estimate was computed from the N-body particles and it is expected to be an upper limit for the actual infall velocity of the secondary cluster gas which decreases as it is stripped from its gravitational potential. Moreover, in order to compute v_{bal} , we have assumed that the secondary cluster peak density remains constant throughout the merger. If we keep these considerations in mind, we note that there is a trend for cooling flows to survive in cases where $v_s \leq v_{bal}$ within some radius. One exception appears to be #4 which is classified as a strong disruption (Table 1) but we note that even in this case, the final cooling time is less than 2 Gyrs which suggests the flow will quickly re-establish. Therefore, this plot suggests that substantial amounts of secondary cluster gas manage to penetrate into the cluster cooling core only when the ram pressure is larger than the local cooling flow thermal pressure. Note that this ram pressure model is consistent with our results. It also explains naturally why mergers of identical cooling flow clusters and subclusters that differ only in their overall dark matter mass ratio can have different effects on the cooling flow (#4 and #7). The subcluster in the 4:1 mass ratio merger has a greater momentum

than the subcluster in the 16:1 merger (since the 4:1 mergers have a larger infall velocity and core radius) and its gas is therefore able to penetrate and disrupt the primary cooling flow.

Finally, the time-delay (1-2 Gyr) between core crossing and cooling flow disruption further supports the idea that gas processes are ultimately responsible. Previous numerical simulations (e.g., Roettiger et al. 1998; 1999) have shown a 1-2 Gyr delay between core passage and the onset of turbulence which can heat the gas core as it supplies a non-thermal component of pressure support equivalent to $\sim 20\%$ of the core's thermal pressure.

4.2. Later Stages of the Cooling Flow

Will the disrupted cooling flows re-establish themselves? Figure 7 demonstrates that the initial cooling time is critical. For example, mergers #4 and #8 resulted in a relative increase in central cooling time similar to that experienced in mergers #1 and #6 but their cooling times never reach a Hubble time and they even drop a few Gyr by the end of the simulations. Thus only the flows with very short initial cooling times can re-establish themselves after experiencing a significant merger. The severity of the merger also plays a role. For example, merger #1 resulted in disruption and a final central cooling time of ~ 30 Gyr while the identical merger involving lower baryon fraction subclusters (# 2 and #3) caused a relatively mild increase in the cooling time. These mildly affected clusters may also re-establish themselves.

4.3. Radio Sources, Cooling Flows, and Cluster Mergers

Abell 2597 is an interesting cooling flow cluster (cooling rate $\sim 327 M_{\odot}/\text{year}$, Sarazin et al. 1995) which shows some evidence of X-ray and optical substructure (Sarazin et al. 1995, Gómez et al., in preparation) and the presence of a disrupted compact (size ~ 20 kpc) tailed radio source located at the *cluster core* (PKS 2322-122, Owen et al. 1992). Sarazin et al. have examined in detail the radio structure of PKS 2322-122 and determined that one of its jets is sharply bent by more than 90° . In their analysis, they propose several models for the jet bending. One of those models suggests that the bending is caused by the interaction between the jet and a large transversal bulk flow of cluster gas (with velocities ~ 1000 km/s) fueled by a recent cluster merger. Our simulations are not con-

sistent with that dynamical scenario. We find that high velocity flows near the cluster center, such as those required to bend the jets, are inconsistent with the presence of a cooling flow. The mergers that leave the cooling flow unaffected can also produce turbulence and bulk flow gas motions but at much greater distances (> 150 kpc) from the cluster center. Thus, we find that, given the limited spatial resolution of our simulations, large bulk flows (~ 1000 km/s) and cooling flows do not occur within the same region. Therefore, a merger could not maintain a significant cooling flow and produce the gas dynamics needed to bend an extended radio source located at the cooling flow region.

5. SUMMARY AND CONCLUSIONS

We have performed a set of 9 simulations of head-on mergers of two galaxy clusters that include, for the first time, the effects of radiative cooling. The objective of the simulations was to determine how different mergers would affect a cluster cooling flow. The parameter space covered by this study consisted of a range of mass ratios for the two clusters (16:1 and 4:1), a range of overall baryon fractions of the secondary cluster (from 1.2% to 15%), and a range of strengths of the primary cluster cooling flow (100 and 400 M_{\odot}/year). The simulations were performed with a combined Hydrodynamics/N-body code on a grid with a resolution of 20 kpc. The N-body particles were evolved in 3-D while the gas evolution calculations were performed in 2-D because there is symmetry around the merger axis.

We find that some cluster mergers destroy cooling flows while others leave them intact. Our analysis of these results lead us to draw the following three conclusions. First, the destruction of the primary cluster cooling flow depends principally on the ram-pressure of the gas in the infalling cluster. In accordance with this, we found that if all other parameters are kept fixed, the likelihood of disrupting a cooling flow increases as the baryon fraction in the secondary cluster increases. We attribute the disruption to two factors linked to the gas dynamics of the merger; the ram-pressure of the subcluster gas is able to displace the high-density gas in the cooling core as well as heating it through adiabatic compression, shocks and turbulence. Second, the time-scale on which a new cooling flow re-establishes itself depends on the initial cooling time of the cluster as well as on the severity of

the merger. The post-merger cooling times of initially short cooling-time flows are less than a Hubble time and thus they may re-establish themselves quickly. Third we note that, in the case of disruption, there is a lag of at least 1-2 Gyr between the epoch of the merger (when the dark matter cores cross) and the point at which the central cooling time increases to the Hubble time. These last two conclusions have important consequences for interpreting observational determinations of the frequency of cooling flow and substructure occurrence. Any cooling flow cluster involved in a merger will exhibit some degree of substructure *and* appear to have a cooling flow for at least 1-2 Gyrs after core-passage. Furthermore, if the initial cooling time is very short (10-40 times less than a Hubble time), then mergers of the type discussed here will continue to be identified as cooling flows on the basis of their cooling times.

The work presented here is only preliminary in nature since significant parameter space is left to be explored. We have not addressed details of the gas and dark matter core structure, both of which could be important. Recent gravitational lensing experiments indicate that central dark matter distributions may be considerably more concentrated (i.e. cuspy) than depicted here. Furthermore, cosmological numerical simulations of the evolution of dark matter halos support the steep models for the dark matter (e.g., Navarro, Frenk, & White 1997). In general, we believe that a steeper profile could enhance the survivability of the cooling flow region during the merger due to the deeper gravitational potential and/or favor a rapid re-start of a disrupted cooling flow. On the other hand, the deep gravitational potentials generated by these steep profiles could also lead to more violent head-on mergers. In this respect, the degree of disruption may be enhanced. However, another difference between a NFW type of profile and our models is that in these steeper models the baryon fraction increases as a function of radius. Since the subcluster will encounter a larger amount of gas during its fall, it is very likely that it will not penetrate as deep as in our models and stop further from the cooling flow center. Another interesting case not addressed in our study is the merger of two cooling flow clusters. As our simulations show, any process or situation that increases the ram pressure of the infalling clusters will have a disruptive effect on the cooling flows. Thus, the merger of two cooling flows will probably disrupt both cooling flows. We have also not ad-

ressed off-axis mergers (Roettiger et al. 1998; Ricker 1998). Cooling flow survivability could be greatly enhanced if the merger is only marginally off-axis. Finally, there are always potential resolution effects. To this end, future work will employ higher resolution, fully 3-dimensional simulations which will allow off-axis merger, cuspier dark matter distributions and a more detailed look at the roll of post-merger turbulence in cooling flow disruption.

This work was partially supported by a NASA Long Term Space Astrophysics grant NAGW-3152 and NSF grants AST93-17596 and AST98-96039 to JOB. PLG would like to acknowledge additional support received by a NASA grant NAG5-3432 and CL and PLG also acknowledge the support from NASA grant NAG5-3842. We would like to thank the Pittsburg Supercomputer Center TAC committee for granting time to perform our simulations on the C90 and the College of Engineering at New Mexico State University for access to their Cray YMP-EL, W. Gibbs for guiding discussions related to the Poisson equation, Anatoly Klypin for useful discussions about N-body, shock, and entropy evolution, C. Sarazin for insightful comments regarding the project, and an anonymous referee for very detailed and lucid comments and suggestions. ZEUS-3D was developed and maintained by the Laboratory of Computational Astrophysics (LCA) at the National Center for Supercomputing Applications (NCSA).

REFERENCES

- Allen, S. W., Fabian, A. C., Edge, A. C., Böhringer, H., & White, D. A. 1995, *MNRAS*, 275, 741
- Allen, S. W., Fabian, A. C., Edge, A. C., Bautz, M. W., Furuzawa, A., & Tawara, Y. 1996, *MNRAS*, 283, 263
- Binney, J. & Tremaine, S. 1987, *Galactic Dynamics* (Princeton: Princeton University Press)
- Birkinshaw, M. 1979, *MNRAS*, 187, 847
- Bond, J.R., Kofman, L., & Pogosyan, D. 1996, *Nature*, 380, 603
- Böhringer, Neumann, D. M., Schindler, S., & Kraankorteweg, R. C. 1996, *ApJ*, 467, 1680
- Briel, U. G. & Henry, J. P. 1994, *Nature*, 372, 439
- Buote, D. A. & Tsai, J. C. 1996, *ApJ*, 458, 27
- Burns, J. O., Roettiger, K., Ledlow, M., & Klypin, A. 1994, *ApJ*, 427, L87
- Burns, J. O., Roettiger, K., Pinkney, J., Perley, R. A., Owen, F. N., & Voges, W. 1995, *ApJ*, 446, 583
- Burns, J. O. 1998, *Science*, 280, 400
- Clarke, D. A. 1990, *BAAS*, 22, 1302
- Colberg, J.M., White, S.D.M., Jenkins, A., & Pearce, F.R. 1999 *MNRAS*, in press
- Colless, M., Saglia, R. P., Burstein, D, Davies, R., McMahan, R. K., & Wegner, G. 1999, in *Cosmic Flows*, eds. S. Courteau, M. Strauss, J. Willick, preprint astro-ph/9909062
- Crawford, C. S., Edge, A. C., Fabian, A. C., Allen, S. W., Böhringer, Ebeling, H., McMahon, R. G., and Voges, W. 1995, *MNRAS*, 274, 75
- Davis, D. & Mushotzky, R. 1993, *AJ*, 105, 409
- Donahue M., Stocke J. T., & Gioia, I. M. 1992, *ApJ*, 385, 49
- Edge, A. C. & Stewart, G. C. 1991, *MNRAS*, 252, 428
- Edge, A.C., Stewart, G.C., & Fabian, A.C. 1992, *MNRAS*, 258, 177
- Edge, A.C. 1997, in *ASP Conf. Ser. 115, Galactic Cluster Cooling Flows*, ed. N. Soker (San Francisco: ASP), 59
- Eisenstat, S., Elman, H. C., & Schultz, M. H. 1983, *Siam. J. Numer. Anal.*, 20, 345
- Evrard, A., Mohr, J., Fabricant, D., & Geller, M. 1993, *ApJ*, 419, 9
- Fabian, A. C. & Daines, S. J. 1991, *MNRAS*, 252, 17
- Fabian, A. C. 1994, *ARA&A*, 32, 277
- Gunn, J. 1978, in *Observational Cosmology*, eds. A. Ameder, J. Marinnet, & G. Tammann (Geneva: Geneva Observatory)
- Heckman, T. M., Baum, S. A., Van Breugel, W. J. M., & McCarthy, P. 1989, *ApJ*, 338, 48
- Hernquist, L. 1987, *ApJS*, 64, 715
- King, I. R. 1966, *AJ*, 61, 74
- Knight, P.A. & Ponman, T.J. 1997, *MNRAS*, 289, 955
- Markevitch, M. L. 1996, *ApJ*, 465, L1
- Markevitch, M., Forman, W.R., Sarazin, C.L., & Vikhlinin, A. 1998, *ApJ*, 503, 77
- Markevitch, M., Sarazin, C. L., & Vikhlinin, 1998b, preprint (astro-ph/9812005)
- McGlynn, T.A. & Fabian, A.C. 1984, *MNRAS*, 208, 709
- Mohr, J., Fabricant, D., & Geller, M. 1993, *ApJ*, 413, 492
- Mohr, J., Evrard, A., Fabricant, D., & Geller, M. 1995, *ApJ*, 447, 8
- Mulchaey, J. S, Davis, D., Mushotzky, R., & Burnstein, D. 1996, *ApJ*, 456, 80
- Navarro, J. F., Frenk, C. S., & White, S. D. M. 1997, *ApJ*, 490, 493
- Oppe, T. C., Joubert, W. D., & Kincaid, D. R. 1988, in *NSPCG User's Guide*, Center for Numerical Analysis, The University of Texas at Austin
- Owen, F., White, R., & Burns, J. O. 1992, *ApJS*, 80, 501

- Pearce, F. R., Thomas, P. A., & Couchman, H. M. P. 1994, MNRAS, 268, 953
- Peres, C.B., Fabian, A.C., Edge, A.C., Allen, S.W., Johnstone, R.M., & White, D.A. 1998, MNRAS, 298, 416
- Raymond, J. C. & Smith, B. W. 1977, ApJS, 35, 419
- Richstone, D., Loeb, A. & Turner, E. L. 1992, ApJ, 393, 477
- Ricker, P. M. 1998, ApJ, 496, 670
- Rizza, E., Burns, J. O., Ledlow, M., Owen, F.N., Voges, W., & Bliton, M. 1998, MNRAS, 301, 328
- Roettiger, K., Burns, J., Loken, C. 1993, ApJ, 407, L53
- Roettiger, K., Burns, J.O., Loken, C. 1996, ApJ, 473, 651
- Roettiger, K., Burns, J. O., & Pinkney, J. 1995, ApJ, 453, 634
- Roettiger, K., Loken, C. & Burns, J. O. 1997, ApJS, 109, 307
- Roettiger, K., Stone, J., & Mushotzky, R. 1998, ApJ, 493, 62
- Roettiger, K. Stone, J., & Burns, J. O. 1999, ApJ, 518, 594
- Sarazin, C.L, Burns, J.O., Roettiger, K., & McNamara, B.R. 1995, ApJ, 447, 559
- Schindler, S & Müller, E. 1993, A&A, 272, 137
- Stewart, G. C., Fabian, A. C., Jones, C., & Forman, W. 1984, ApJ, 285, 1
- Stone, J. M. & Norman, M. L. 1992, ApJS, 80, 791
- Thomas, P. A., Fabian, A. C., & Nulsen, E. J. 1987, MNRAS, 228, 973
- Westbury, C. R. & Henriksen, R. N. 1992, ApJ, 338, 64
- White, D.A., Jones, C., & Forman, W. 1997, MNRAS, 292, 419
- White, S. D. M., Briel, U. G., & Henry, J. P. 1993, MNRAS, 261, 8
- White, R. E. and Sarazin, C. L. 1987, ApJ, 318, 629
- White, S. D. M. & Silk, J. 1980, ApJ, 241, 864

Fig. 1.— Radial gas density (top) and temperature profiles (bottom) for the $400M_{\odot}/\text{year}$ (asterisks) and the $100M_{\odot}/\text{year}$ (diamonds) steady-state cooling flows.

Fig. 2.— Plot of the evolution of the gravitational potential minimum as a function of time for the 1:4 (solid line) and 1:16 (dashed line) mass ratio mergers. The time is relative to the time of core crossing. Note that the most dramatic increase (absolute) in the gravitational potential lasts for about 1 Gyr.

Fig. 3.— Contours of the logarithm of the gas density for run #8. The grey scale maps represent the logarithm of the density of the passive scalar that traces the subcluster gas. Note that the times are relative to the time of core crossing and that the axes are labeled in units of Mpc. The same contour levels were applied to all the 6 panels in this figure.

Fig. 4.— Plot of the gas density along the merger axis for the merger #8 (left) and merger #7 (right). The epochs correspond to (from top to bottom) 0.25, 1.0, and 5.5 Gyrs. The shaded plot corresponds to the secondary cluster passive scalar. Furthermore, the vertical dotted line shows the location of the gravitational potential minimum in each epoch. Note that for the same epoch, the secondary gas penetrates deeper and in larger quantities in merger #8 than in merger #7. The x axis is labeled in units of 20 kpc. The time is relative to the moment of core crossing.

Fig. 5.— Contours of the logarithm of the gas density for run #7. The grey scale maps represent the logarithm of the density of the passive scalar that traces the subcluster gas. Note that the times are relative to the time of core crossing and that the axes are labeled in units of Mpc. The same contour levels were applied to all the 6 panels in this figure.

Fig. 6.— Color plots of the gas temperature distribution at different epochs during the merger for the simulation #8 (top) and #7 (bottom). The merger epochs correspond to (from left to right) 0.25, 1.0, and 5.5 Gyrs relative to the time of core crossing. The cooling flow is the dark region located at the core of the primary cluster. All of these panels have the same color scale that shows the hottest regions in white. The axes are labeled in units of Mpc.

Fig. 7.— Plot of the evolution of the primary cluster cooling time as a function of time for the 1:4 mass

ratio mergers (bottom) and 1:16 mass ratio mergers (top). The different lines represent the different mergers with different cooling flow strengths and baryon mass fraction as indicated. The numbers in between parenthesis correspond to the labels in Table 1. The time is relative to the moment of core crossing.

Fig. 8.— Plot of the evolution of the primary cluster temperature as a function of time for the 1:4 mass ratio mergers (bottom) and 1:16 mass ratio mergers (top). The different lines represent the different mergers with different cooling flow strengths and baryon mass fraction as indicated. The numbers in between parenthesis correspond to the labels in Table 1. The time is relative to the moment of core crossing.

Fig. 9.— Plot of v_s and v_{bal} as a function of radius for the 1:4 mass ratio mergers (right) and 1:16 mass ratio mergers (left). The symbols represent the different types of mergers (see Table 1). The solid line with no symbols in each panel represents the v_{ram} as computed from the relative velocities of the N-body particles belonging to each cluster.

TABLE 1
SIMULATION DATA

label	mass ratio	# of particles		r_c (kpc)		cooling flow (M_\odot/year)	central density (cm^{-3})		baryon fraction %	T (keV)	level of disruption of CF
		P	S	P	S		P	S			
1	1:4	30000	7500	250	157	100	0.0015	15.0	6.6	strong	
2	1:4	30000	7500	250	157	100	0.0006	5.0	6.6	mild	
3	1:4	30000	7500	250	157	100	0.0003	2.5	6.6	mild	
4	1:4	30000	7500	250	157	400	0.0006	5.0	6.6	strong	
5	1:16	30000	1875	250	99	100	0.0006	5.0	2.6	mild	
6	1:16	30000	1875	250	99	100	0.0012	10.0	2.6	strong	
7	1:16	30000	1875	250	99	400	0.0006	5.0	2.6	none	
8	1:16	30000	1875	250	99	400	0.0012	10.0	2.6	strong	
9	1:16	30000	1875	250	99	400	0.0001	1.2	2.6	none	

NOTE.—P and S refer to the values in the primary and secondary cluster respectively.

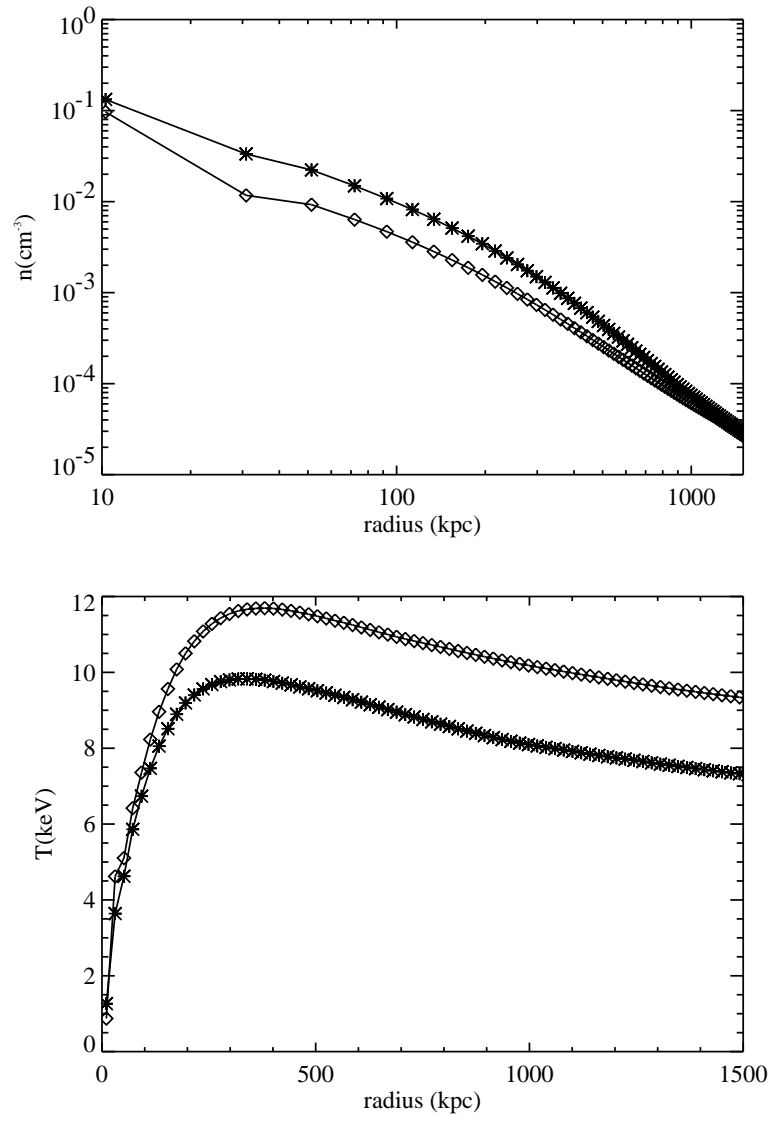


Figure 1.

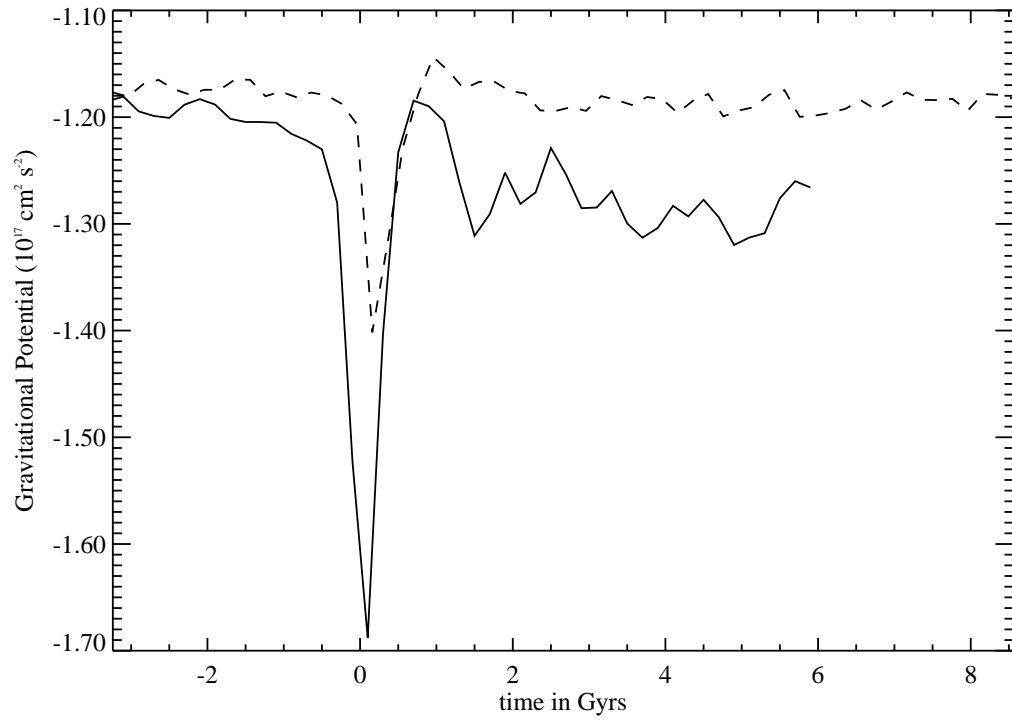


Figure 2.

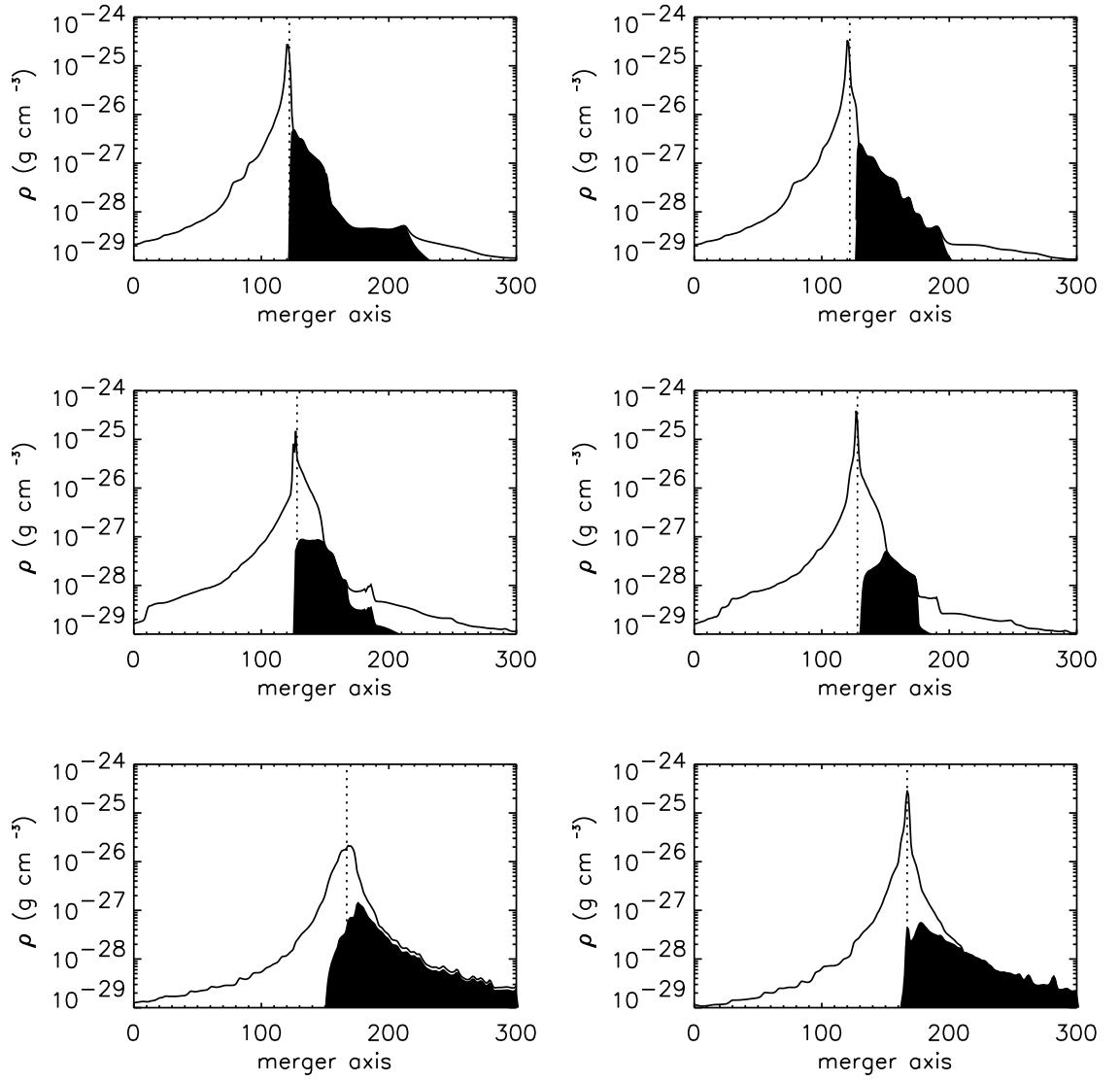


Figure 4.

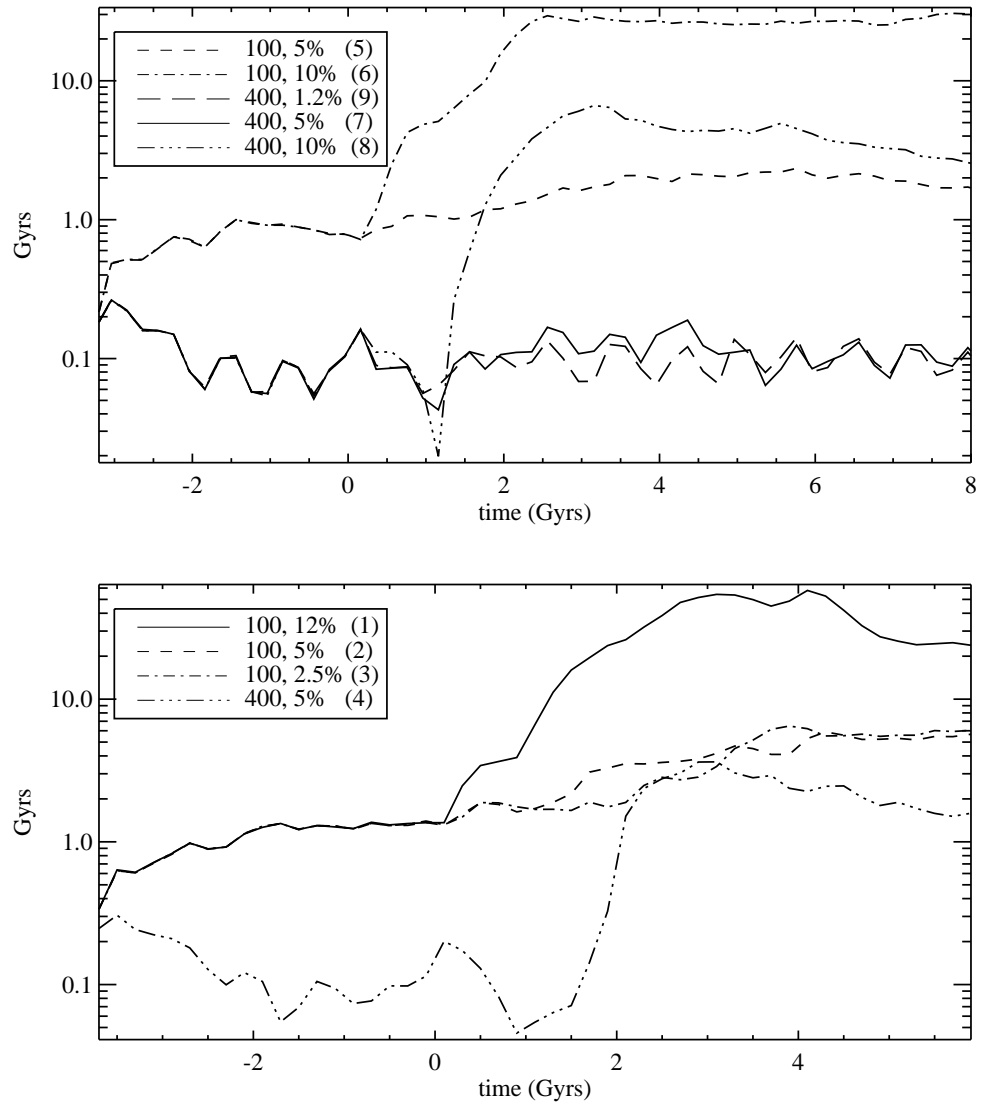


Figure 7.

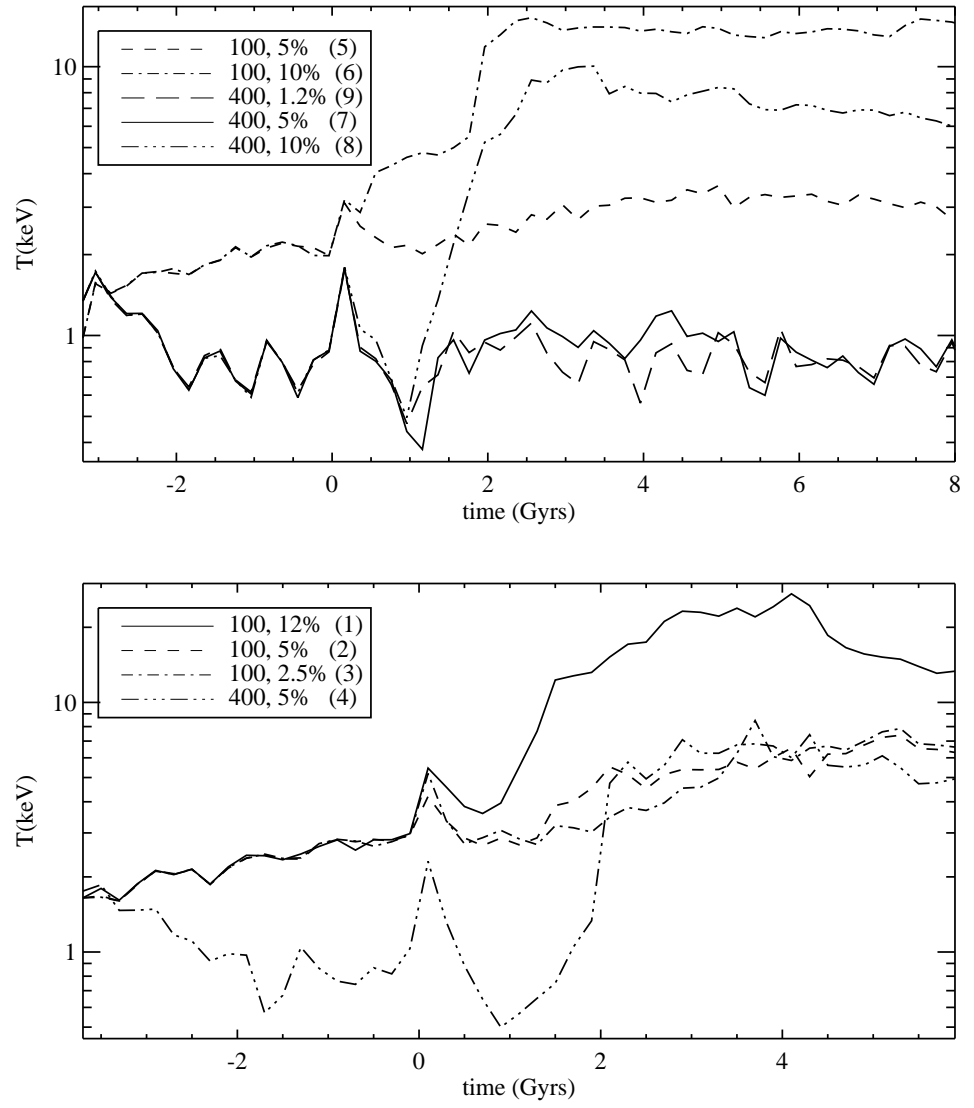


Figure 8.

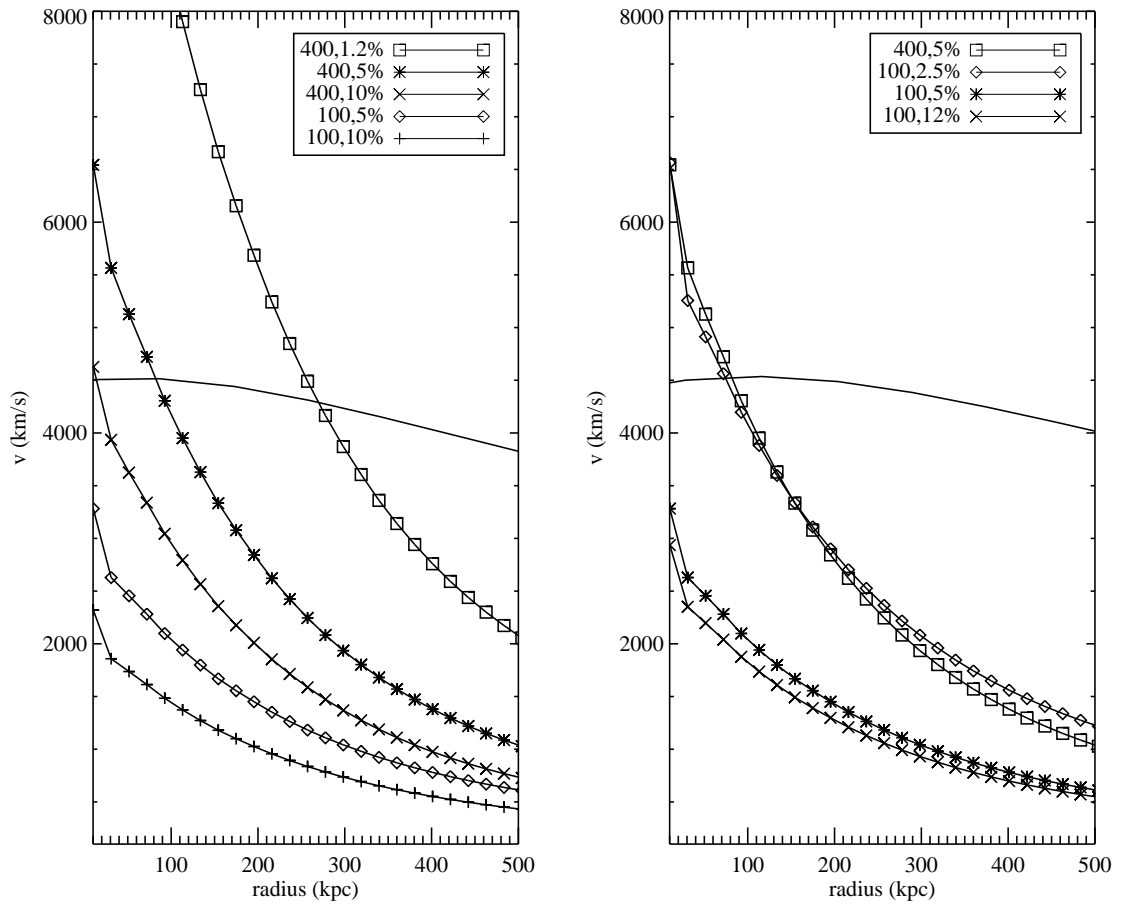


Figure 9.

This figure "f3l.jpg" is available in "jpg" format from:

<http://arxiv.org/ps/astro-ph/0009465v1>

This figure "f51.jpg" is available in "jpg" format from:

<http://arxiv.org/ps/astro-ph/0009465v1>

This figure "f6l.jpg" is available in "jpg" format from:

<http://arxiv.org/ps/astro-ph/0009465v1>